The absorption tunability and enhanced electromagnetic coupling of terahertz-plasmons in grating-gate AlN/GaN plasmonic device

Lin Wang,[1] Xiaoshuang Chen,[1,*] Weida Hu,[1,3] Anqi Yu[1], Shaowei Wang,[1,2] and Wei Lu[1]

[1]*National Laboratory for Infrared Physics, Shanghai Institute of Technical Physics, Chinese Academy of Sciences, Shanghai 200083, China*

[2]*Shanghai Advanced Research Institute, Chinese Academy of Sciences, Shanghai 200083, China*

[3]*wdhu@mail.sitp.ac.cn*

[*]*xschen@mail.sitp.ac.cn;*

Abstract: This paper describes the dynamic interaction between plasmons in a two dimensional electron gas system under electrical tuning to the high density regime in AlN/GaN high electron mobility transistor. The results demonstrate an enhanced resonance when the two plasmons are commonly excited, during which the potentially splitting phenomenon of such resonance is explored in detail. An asymmetrical plasmon possess wide frequency tunability has also been demonstrated in the AlN/GaN system, on the contrary, the results also indicate a finite tunable regime of symmetrical-plasmons as limited by the coupling strength between such plasmons. For the devices with narrow gate-fingers, significant near-field enhancement can be obtained due to the strong cavity pumping of electromagnetic energy. These properties may have important applications including high-responsivity quantum-dot detection systems, THz modulator etc.

OCIS codes: (050.2770) Gratings; (250.5403) Plasmonics; (040.2235) Far infrared or terahertz; (040.0040) Detectors.

References and links

1. N. Pala and M. S. Shur, "Plasmonic terahertz detectors for biodetection," Electron. Lett. **44**(24), 1391–1392 (2008).
2. M. S. Shur, "Silicon and nitride FETs for THz sensing," Proc. SPIE **8031**, 80310J (2011).
3. T. A. Elkhatib, V. Y. Kachorovskii, W. J. Stillman, D. B. Veksler, K. N. Sala, X.-C. Zhang, and M. S. Shur "Enhanced plasma wave detection of terahertz radiation using multiple high electron-mobility transistors connected in series," IEEE Trans. Microave Theory Tech. **58**(2), 331–339 (2010).
4. E. A. Shaner, M. C. Wanke, A. D. Grine, S. K. Lyo, J. L. Reno, and S. J. Allen, "Enhanced responsivity in membrane isolated split-grating-gate plasmonic terahertz detectors," Appl. Phys. Lett. **90**(18), 181127 (2007).
5. S. Kim, J. D. Zimmerman, P. Focardi, A. C. Gossard, D. H. Wu, and M. S. Sherwin, "Room-temperature terahertz detection based on bulk plasmons in antenna-coupled GaAs field effect transistors," Appl. Phys. Lett. **92**(25), 253508 (2008).
6. W. Knap, S. Nadar, H. Videlier, S. Boubanga-Tombet, D. Coquillat, N. Dyakonova, F. Teppe, K. Karpierz, J. Łusakowski, M. Sakowicz, I. Kasalynas, D. Seliuta, G. Valusis, T. Otsuji, Y. Meziani, A. E. I. Fatimy, S. Vandenbrouk, K. Madjour, D. Théron, and C. Gaquière, "Field effect transistors for terahertz detection and emission," J. Infrared Milli Terahz Waves. **32**(5), 618–628 (2011).
7. W. Knap, M. Dyakonov, D. Coquillat, F. Teppe, N. Dyakonova, J. Łusakonski, K. Kavpierz, M. Sakowicz, G. Valusis, D. Seliuta, I. Kasalynas, A. E. I. Fatimy, Y. M. Meziani, and T. Otsuji, "Field effect transistors for terahertz detection: physics and first imaging applications," J. Infrared Milli Terahz Waves. **30**, 1319–1337 (2009).
8. G. C. Dyer, G. R. Aizin, J. L. Reno, E. A. Shaner, and S. J. Allen, "Novel tunable millimeter-wave grating-gated plasmonic detectors," IEEE J. Sel. Top. Quantum Electron. **17**(1), 85–91 (2011).
9. S. J. Allen, D. C. Tsui, and R. A. Logan, "Observation of the two-dimensional plasmon in silicon inversion layers," Phys. Rev. Lett. **38**(17), 980–983 (1977).
10. M. Dyakonov and M. S. Shur, "Detection, mixing and frequency multiplication of terahertz radiation by two-dimensional electronic fluid," IEEE Trans. Electron. Dev. **43**(3), 380–387 (1996).
11. W. Knap, F. Teppe, N. Dyakonova, D. Coquillat, and J. Łusakowski, "Plasma wave oscillations in nanometer field effect transistors for terahertz detection and emission," J. Phys. Condens. Matter **20**(38), 384205 (2008).

#182409 - $15.00 USD Received 2 Jan 2013; revised 17 Mar 2013; accepted 19 Apr 2013; published 25 Apr 2013

12. E. A. Shaner, M. Lee, M. C. Wanke, A. D. Grine, J. L. Reno, and S. J. Allen, "Single-quantum-well grating-gated terahertz plasmon detectors," Appl. Phys. Lett. **87**(19), 193507 (2005).
13. M. Dyakonov and M. S. Shur, "Shallow water analogy for a ballistic field effect transistor: new mechanism of plasma wave generation by dc current," Phys. Rev. Lett. **71**(15), 2465–2468 (1993).
14. V. V. Popov, D. M. Ermolaev, K. V. Maremyanin, N. A. Maleev, V. E. Zemlyakov, V. I. Gavrilenko, and S. Yu. Shapoval, "High-responsivity terahertz detection by on-chip InGaAs/GaAs field-effect-transistor array," Appl. Phys. Lett. **98**(15), 153504 (2011).
15. V. V. Popov, O. V. Polischuk, T. V. Teperik, X. G. Peralta, S. J. Allen, N. J. M. Horing, and M. C. Wanke, "Absorption of terahertz radiation by plasmon modes in a grid-gated double-quantum-well field-effect transistor," J. Appl. Phys. **94**(5), 3556–3562 (2003).
16. X. G. Peralta, S. J. Allen, M. C. Wanke, N. E. Harff, J. A. Simmons, M. P. Lilly, J. L. Reno, P. J. Burke, and J. P. Eisenstein, "Terahertz photoconductivity and plasmon modes in double-quantum-well field-effect transistors," Appl. Phys. Lett. **81**(9), 1627–1629 (2002).
17. A. V. Muravjov, D. B. Veksler, X. Hu, R. Gaska, N. Pala, H. Saxena, R. E. Peale, and M. S. Shur, "Resonant terahertz absorption by plasmons in grating-gate GaN HEMT structures," Proc. SPIE **7311**, 73110D (2009).
18. M. I. Dyakonov and M. S. Shur, "Plasma wave electronics: novel terahertz devices using two dimensional electron fluid, " IEEE Trans. Electron Devices **43**(10), 1640–1645 (1996).
19. E. A. Shaner, A. D. Grine, J. L. Reno, M. C. Wanke, and S. J. Allen, "Next-generation detectors—Plasmon grating-gate devices have potential as tunable terahertz detectors," Laser Focus World **44**, 131–133 (2008).
20. V. V. Popov, A. N. Koudymov, M. S. Shur, and O. V. Polischuk, "Tuning of ungated plasmons by a gate in the field-effect transistor with two-dimensional electron channel," J. Appl. Phys. **104**(2), 024508 (2008).
21. R. E. Peale, H. Saxena, W. R. Buchwald, G. C. Dyer, and S. J. Allen, Jr., "Grating-gate tunable plasmon absorption in InP and GaN based HEMTs," Proc. SPIE **7311**, 73110I, 73110I-6 (2009).
22. E. A. Shaner, A. D. Grine, M. C. Wanke, M. Lee, J. L. Reno, and S. J. Allen, "Far-Infrared spectrum analysis using plasmon modes in a quantum-well transistor," IEEE Photon. Technol. Lett. **18**(18), 1925–1927 (2006).
23. T. A. Elkhatib, V. Y. Kachorovskii, W. J. Stillman, S. Rumyantsev, X.-C. Zhang, and M. S. Shur, "Terahertz response of field-effect transistors in saturation regime," Appl. Phys. Lett. **98**(24), 243505 (2011).
24. A. El Fatimy, F. Teppe, N. Dyakonova, W. Knap, D. Seliuta, G. Valušis, A. Shchepetor, Y. Roelens, S. Bollaert, A. Cappy, and S. Rumyantsev, "Resonant and voltage-tunable terahertz detection in InGaAs/InP nanometer transistors," Appl. Phys. Lett. **89**(13), 131926 (2006).
25. F. Teppe, M. Orlov, A. E. I. Fatimy, A. Tiberj, W. Knap, J. Torres, V. Gavrilenko, A. Shchepetov, Y. Roelens, and S. Bollaert, "Room temperature tunable detection of subterahertz radiation by plasma waves in nanometer InGaAs transistors," Appl. Phys. Lett. **89**(22), 222109 (2006).
26. A. V. Muravjov, D. B. Veskler, V. V. Popov, O. V. Polischuk, N. Pala, X. Hu, R. Gaska, H. Saxena, R. E. Peale, and M. S. Shur, "Temperature dependence of plasmonic terahertz absorption in grating-gate gallium-nitride transistor structures," Appl. Phys. Lett. **96**(4), 042105 (2010).
27. L. Wang, X. S. Chen, W. D. Hu, and W. Lu, "Spectrum analysis of 2D plasmon in GaN-based high electron mobility transistors," IEEE J. Sel. Top. Quantum Electron. **19**(1), 8400507–8400513 (2013).
28. A. M. Dabiran, A. M. Wowchak, A. Osinsky, J. Xie, B. Hertog, B. Cui, D. C. Look, and P. P. Chow, "Very high channel conductivity in low-defect AlN/GaN high electron mobility transistor structures," Appl. Phys. Lett. **93**(8), 082111 (2008).
29. Y. Cao and D. Jena, "High mobility window for two-dimensional electron gases at ultrathin AlN/GaN heterojunctions," Appl. Phys. Lett. **90**(18), 182112 (2007).
30. T. Zimmermann, D. Deen, Y. Cao, J. Simon, P. Fay, D. Jena, and H. G. Xing, "AlN/GaN isulated-gate HEMTs with 2.3A/mm output current and 480 mS/mm transconductance," IEEE Electron Device Lett. **29**(7), 661–664 (2008).
31. S. Taking, D. MacFarlane, and E. Wasige, "AlN/GaN MOS-HEMTs with thermally grown Al_2O_3 passivation," IEEE Trans. Electron. Dev. **58**(5), 1418–1424 (2011).
32. M. Dyakonov and M. S. Shur, "Current instability and plasma waves generation in ungated two-dimensional electron layers," Appl. Phys. Lett. **87**(11), 111501 (2005).
33. L. Wang, X. S. Chen, W. D. Hu, J. Wang, X.-D. Wang, and W. Lu, "The plasmonic resonant absorption in GaN double-channel high electron mobility transistors," Appl. Phys. Lett. **99**(6), 063502 (2011).
34. L. Wang, X. S. Chen, W. D. Hu, and W. Lu, "The role of ultrathin AlN barrier in the reduction in the hot electron and self-heating effects for GaN-based double-heterojunction high electron mobility transistors," J. Appl. Phys. **108**(5), 054501 (2010).
35. T. Otsuji, M. Hanabe, T. Nishimura, and E. Sano, "A grating-bicoupled plasma-wave photomixer with resonant-cavity enhanced structure," Opt. Express **14**(11), 4815–4825 (2006).
36. V. V. Popov, O. V. Polischuk, W. Knap, and A. El Fatimy, "Broadening of the plasmon resonance due to plasmon-plasmon intermode scattering in terahertz high-electron-mobility transistors," Appl. Phys. Lett. **93**(26), 263503 (2008).
37. V. V. Popov, D. V. Fateev, O. V. Polischuk, and M. S. Shur, "Enhanced electromagnetic coupling between terahertz radiation and plasmons in a grating-gate transistor structure on membrane substrate," Opt. Express **18**(16), 16771–16776 (2010).
38. L. Wang, W. D. Hu, J. Wang, J. Wang, X. D. Wang, S. W. Wang, X. S. Chen, and W. Lu, "Plasmon resonant excitation in grating-gated AlN barrier transistors at terahertz frequency," Appl. Phys. Lett. **100**(12), 123501 (2012).

#182409 - $15.00 USD Received 2 Jan 2013; revised 17 Mar 2013; accepted 19 Apr 2013; published 25 Apr 2013

39. V. V. Popov, O. V. Polishchuk, and W. Knap, "Plasmon-plasmon scattering and giant broadening of the gated plasmon resonance line in a nanometric heterotransistor with a 2D electron channel," Bull. Russ. Acad. Sci., Physics **73**(1), 84–87 (2009).
40. A. Satou, V. Ryzhii, and A. Chaplik, "Plasma oscillations in two-dimensional electron channel with nonideally conducting side contacts," J. Appl. Phys. **98**(3), 034502 (2005).
41. H. Marinchio, J.-F. Millithaler, C. Palermo, L. Varani, L. Reggiani, P. Shiktorov, E. Starikov, and V. Gružinskis, "Plasma resonances in a gated semiconductor slab of arbitrary thickness," Appl. Phys. Lett. **98**(20), 203504 (2011).
42. M. Schubert, T. E. Tiwald, and C. M. Herzinger, "Infrared dielectric anisotropy and phonon modes of sapphire," Phys. Rev. B **61**(12), 8187–8201 (2000).
43. V. V. Popov, G. M. Tsymbalov, and N. J. M. Horing, "Anticrossing of plasmon resonances and giant enhancement of interlayer terahertz electric field in an asymmetric bilayer of two-dimensional electron strips," J. Appl. Phys. **99**(12), 124303 (2006).
44. D. V. Fateev, V. V. Popov, and M. S. Shur, "Transformation of the plasmon spectrum in a grating-gate transistor structure with spatially modulated two-dimensional electron channel," Semiconductors **44**(11), 1406–1413 (2010).

1. Introduction

Since the last decade, terahertz (THz) technology has grown dramatically due to its potential advantage in applications like imaging, medical, security and industrial controls [1,2]. However, the development of sensing systems utilizing THz technology is still at its embryonic stage partly due to the lack of THz detectors of high sensitivity with a wide frequency response at room temperature [2,3]. Recently the field effect transistor (FET) and high electron mobility transistor (HEMT) detectors utilizing two-dimensional (2D) plasmons have been the focus of great interest [4–14]. The nonlinear behavior of collective charge density oscillation (plasmon) in FET and HEMT can lead to the rectification of the ac voltage induced by the incoming THz radiation [10,15,16]. In comparison with the intersubband transitions detectors, the plasmonic devices are more suitable for room temperature operation since the plasmonic excitation does not saturate with temperature [5,13]. Furthermore, the propagation velocity of charge density perturbations is an order of magnitude faster than the transferring velocity of carriers in real-space, which is benefit for the development of real-time THz camera [17–27].

Recently, a large-area slit-grating-gate AlGaN/GaN-based HEMT device possesses wide tunability of resonance absorption at THz frequency due to the high electron density induced by the polarization effect [26,27]. Additionally, the high electron density in the channel of GaN devices can increase the operating frequency of fundamental plasmon and expand the applications of plasmonic devices at THz band. In this paper, the 2D plasmon resonances and relevant dynamics in AlN/GaN HEMT under tuning to the high density regime are considered. The excitation of plasmon resonances in different regions of a channel, their interaction and the absorption tunability are discussed in detail. The relevant dynamics of ungated plasmons in the channel exhibit some properties different from those reported in previous work.

2. Device description and characteristic parameters

An AlN/GaN HEMT structure with 2μm thick GaN buffer layer is shown in Fig. 1 schematically. The structure can be grown on *c*-plane sapphire or SiC substrate by either metal organic chemical vapor deposition or molecular beam epitaxy [28–30]. Room temperature Hall measurements indicate that the 2DEG concentration in the kind device can exceed $3 \times 10^{13}\text{cm}^{-2}$. The mobility is approximately $1200\text{cm}^2/\text{Vs}$ (corresponding to the electron relaxation time $\tau = 0.14\text{ps}$) at room temperature. Further improvement in channel conductivity can be achieved by growing thin Al_2O_3 layer with atomic layer deposition (ALD) or thermal oxide methods as shown by Dabiran *et al*. [28] and Taking *et al*. [31]. The AlN barrier layer and Al_2O_3 layer are 5nm thick each, beyond which the strain relaxation of barrier layer happens [29]. The device fabrication can be completed after deposition and patterning of gate electrodes (the electron-beam lithography can be used for processing the grating-gate [27]).

#182409 - $15.00 USD Received 2 Jan 2013; revised 17 Mar 2013; accepted 19 Apr 2013; published 25 Apr 2013

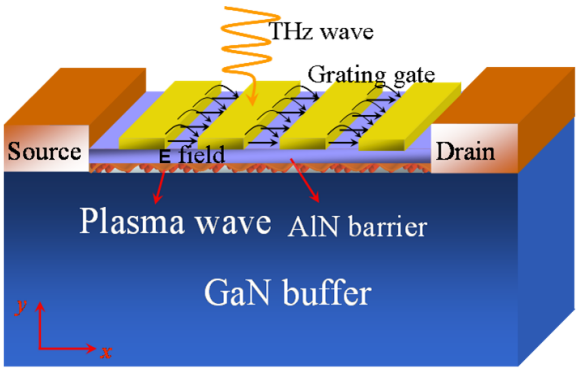

Fig. 1. Schematic structure of slit grating-gate AlN/GaN HEMT. The THz wave is incident vertically from top side with the polarization of electric-field along the x axis. The induced electric field line and plasma waves are shown by the arrows.

It has been known that both the gated and ungated channels can support a plasma wave with dipole oscillation along the channel (symmetrical mode (SM)) [20,32]. Recently, Wang et al. have illustrated that another plasmon with dipole oscillation vertical to the channel can also exist in the gated region of a channel (asymmetrical mode (ASM)), which is the result of electromagnetic interaction between the two surface electrons of the channel [33]. Here, the electromagnetic response of 2DEG in a local approximation is described by Drude conductivity $\sigma(x) = N(x)e^2\tau/m^*(1-i\omega\tau)$, in which m^* is the effective electron mass, τ is the scattering time caused by the phonons, impirities *etc*., e is the elementary charge, $N(x)$ is the sheet electron density along the channel. Generally, the electron density $N(x)$ in the gated region of a channel is different from that in the ungated region, even though there is no electric field added. The electron density distributions can be obtained by solving the Poisson equation as in [34]. With the extracted parameters, the Drude-conductivity is embedded by a convolution method to describe the plasmonic oscillation along the channel of AlN/GaN HEMT [9,20,33,35].

3. Results and discussions

3.1. The gated and ungated SM plasmon resonance absorptions

The electron densities in the gated and ungated region of the channel are about $1.93 \times 10^{13}\text{cm}^{-2}$, and $1.82 \times 10^{13}\text{cm}^{-2}$ under zero gate voltage by self-consistently solving the Possion equation with the polarization charge included in each layer. In Fig. 2, the plasmonic absorption spectra are shown for the device with 1.2μm gate length and different slits between gate fingers. From the figure, we can see that a broad absorption band ranging from 1THz to 16THz can be obtained. The resonant peaks superimposed on top of the background absorption are mainly caused by the excitation of plasmons in the channel. Meanwhile, based on the field-profile under THz excitation, the in-plane dipole distributions of plasmon are displayed in the inset of the figure for better understanding. The dipole distribution of peak a_1 (gated mode) is shown at the upper part of the figure (while the peaks a_2, a_3…are the higher order modes of resonance a with similar dipole distributions but smaller net dipole moment than that of peak a_1), and the dipole distribution of peak b(ungated mode) is shown at the bottom part.

#182409 - $15.00 USD Received 2 Jan 2013; revised 17 Mar 2013; accepted 19 Apr 2013; published 25 Apr 2013

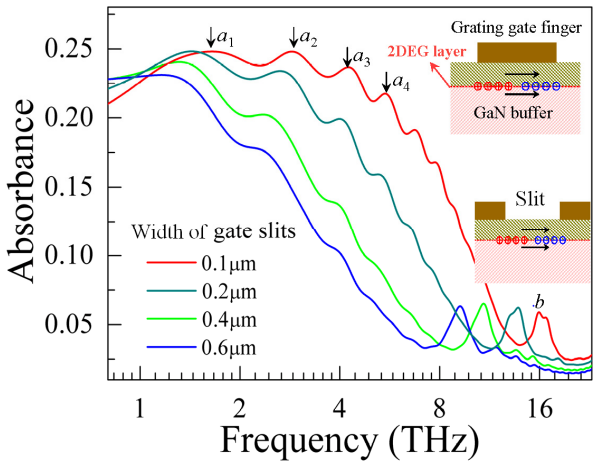

Fig. 2. The spectra of 2D plasmon resonances in the channels of AlN/GaN HEMTs with the width of gate slit spanning from 0.1 to 0.6μm. Two categories of plasmonic peaks *a* (a_1, a_2, a_3…) and *b* are indicated. Insets show the dipole oscillation of gated (upper one) and ungated plasmons (lower one) in the gated and ungated channels, respectively.

By eliminating the Drude background absorption [9,36], it can be found that the higher order plasmon resonance of peak *a* is strengthened successively when the size of gate slits decreases. For example, the plasmon resonances up to 6th order can be excited in the device with 0.1μm-slit, which is benefiting from the strong coupling between THz radiation and plasmons. Hence more energy can be transferred from external radiation to the 2D plasmons, and increase the amplitude of charge oscillating in the channel [37]. The dispersion relations of the plasmons in the gated and ungated regions of channel follow the rules as given in [17,20,27,38],

$$\omega_p = sk_1 = \sqrt{\frac{e^2 n_s d}{\varepsilon_0 \varepsilon_r m^*}} k_1 \quad \text{for gated plasmon} \tag{1}$$

$$\omega_p = \sqrt{\frac{e^2 n_s k_2}{\varepsilon_0 (1+\varepsilon_2) m^*}} \quad \text{for ungated plasmon} \tag{2}$$

in which the condition of the plasma wave vector $k_{1,2}d \ll 1$ can be satisfied in our structure, and n_s is the sheet electron density in the channel, ε_0 is the permittivity of vacuum, and ε_r and ε_2 are the relative dielectric constant of barrier slab and buffer layer, respectively. For a narrow slit grating gate, the wave vector k_1 satisfies the selection rule $2\pi n/L$ (n = 1, 2, 3…), L is the grating period. The mode indexes n of resonances a_1, a_2, a_3…are 1 (fundamental mode), 2 (second order mode), 3 (third order mode)…, respectively, and their frequency interval Δf remains almost constant about 1.3THz.

By increasing the slit-width, the resonant peaks of higher order gated-plasmons become broader and are smeared out alternatively due to several potential mechanisms: i) non-radiative decay of gated plasmon resonance as reported in [36], (ii) the poor coupling efficiency between plasmons and THz radiation for the higher order plasmons with smaller net dipole. However, there may be one exception if the frequencies of gated and ungated plasmon approach with each other, the anti-crossing regime (such regime refers to the plasmon resonant excitation in adjacent channels which have different dimensions or dielectric environment). Popov et al. have predicted that splitting of the resonant peaks may take place when the gated and ungated plasmons are near resonance each other [36,39]. For wider gate-slit, the frequency of ungated plasmons decreases and approaches to that of gated

#182409 - $15.00 USD Received 2 Jan 2013; revised 17 Mar 2013; accepted 19 Apr 2013; published 25 Apr 2013

plasmons. However, the rapidly overdamping of higher order gated plasmons makes the phenomenon unobservable.

3.2. The interaction between gated and ungated SM plasmons at the anti-crossing regime

For better understanding the interaction between gated and ungated SM plasmons at the anti-crossing regime, we turn our attention to the plasmon resonance in the devices with different dimensions and electron densities. Figures 3(a) and 3(b) show the absorption spectra of devices with 1.2μm gate length and 2μm slit, and 0.5μm gate length and 0.4μm slit, respectively. Two different mobility values are used in Fig. 3 (1200cm^2/Vs and 3000 cm^2/Vs in Fig. 3(a), 3000cm^2/Vs and 5000 cm^2/Vs in Fig. 3(b)). The higher value is utilized to reduce the plasmon resonance linewidth caused by the dissipative damping. It is observed that some additional peaks are growing up with the larger mobility (green dotted line in Fig. 3(a)). Further, the resonance peaks around 4.9THz (b_1) and 8.2THz (b_2) (green dotted line in Fig. 3(a)) are caused by the fundamental and second order ungated plasmons. It can be found that the frequency of the fundamental mode is about 2.3 times smaller than that with the 0.4μm gate slit (red dashed line in Fig. 3(a)) in accordance with the dispersion relation given in Eq. (2), while the higher order gated mode is so weak that we do not identify any abnormal phenomena. Stronger gated plasmon resonance can be found in Fig. 3(b) with some different parameters. The second order gated plasmon resonance (a_2) can be clearly visible at around 5.6THz (solid and dotted lines). In similar to the situation in [40], the second order is damped out when the electron density ratio between ungated and gated channel is around 0.6~0.8 (plasma oscillation spreading out much easier over the side of channels). According to the Eq. (1), the third order gated plasmon resonance should be around 8.5THz approaching the ungated plasmon resonance. To our interests, the resonant peak at this frequency (dashed line in Fig. 3(b)) is extraordinary strong as compared with lower order modes (solid and dotted lines), which is completely different from those in Fig. 2.

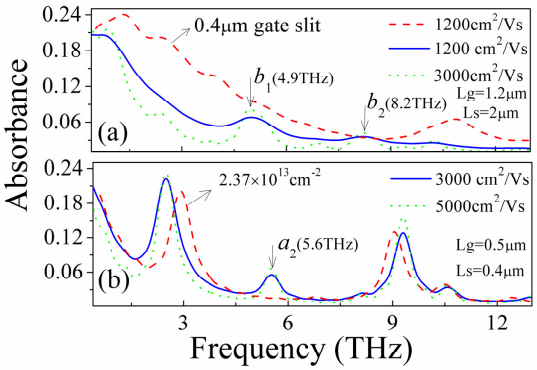

Fig. 3. Plasmonic absorption spectra of the devices with different charge densities and structural sizes: (a) 1.2μm gate length and 2μm slit, blue solid and green dotted lines correspond to the lower mobility 1200cm^2/Vs, and higher mobility 3000 cm^2/Vs, respectively; the spectrum of the device with 0.4μm slit and 1.2μm gate length from Fig. 2 is also shown (red dashed line) for the convenience in comparison; (b) 0.5 μm gate length and 0.4μm slit, blue solid and green dotted lines correspond to lower mobility 3000cm^2/Vs and higher mobility 5000cm^2/Vs, respectively; the spectrum of the device with higher density 2.37 × 10^{13}cm^{-2} in gated channel is also shown for the convenience in comparison (red dashed line). The sheet electron densities, if not specified, are 1.93 × 10^{13}cm^{-2}, 1.82 × 10^{13}cm^{-2} in the gated and ungated channels, respectively. The peaks b_1 and b_2 in the upper panel are the fundamental and second order ungated plasmon resonances, and the peak a_2 in the lower panel is the second order gated plasmon resonance. Ls is the width of gate slit, Lg is the length of gate finger.

In order to understand better, the devices both with and without gratings are tried. Figure 4(a) shows the absorption spectra of devices with different electron densities in the ungated region of channel. In the meantime, the plasmonic spectra of devices without the gate are shown in Fig. 4(b). The purpose is to reduce the frequency-interval between gated and

#182409 - $15.00 USD Received 2 Jan 2013; revised 17 Mar 2013; accepted 19 Apr 2013; published 25 Apr 2013

ungated plasmons, and then reveal the intrinsic physics of plasmon inter-mode interaction at the anti-crossing regime. Still, the splitting of plasmon resonance does not occur at the anti-crossing regime, which is around 6THz or 8THz for the device with or without gate. Instead, only a single resonant peak with the enhanced resonant strength can be observed.

It can be clearly seen that resonances S_1 and S_2 or S_3 and S_4 are excited nearly independently in the channel even though the spreading of electric field causes energy-loss or forced plasmonic oscillation along the adjacent channels (Fig. 4(c)). When approaching the anti-crossing regime, energy-loss can be reduced because the oscillating charges at the adjacent channels can be induced not only by the plasmon scattering but also by the incoming THz wave. As a result, the plasmon resonant enhancement takes places in Figs. 4(a) and 4(b). The fact that the splitting phenomenon of plasmon resonance at the anti-crossing regime does not occur, may be due to (a) the in-phase charge oscillating across the boundaries between gated and ungated channels, or (b) no dipole moment being formed at these boundaries for hybridization of the plasmons. It has been indicated that the splitting of plasmon resonance is related to the different dipole distributions, as shown in [33].

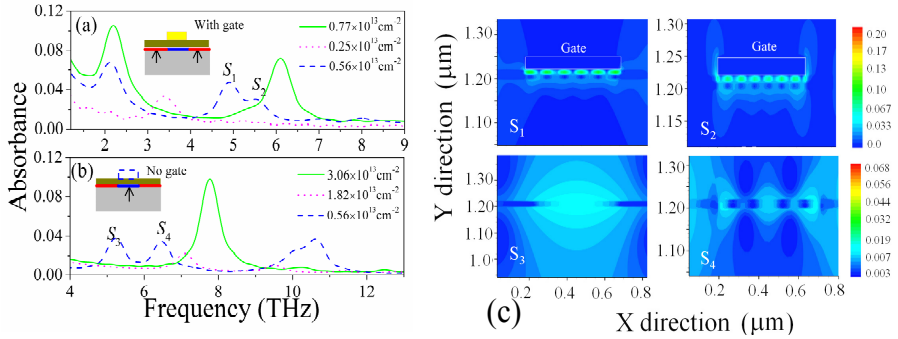

Fig. 4. The plasmonic spectra of the devices with (a) and without (b) gate electrodes added. (a) with gate finger, but different sheet electron densities in the ungated channel, 0.77×10^{13}cm^{-2} (green solid line), 0.25×10^{13}cm^{-2} (red dotted line), 0.56×10^{13}cm^{-2} (blue dashed line); the sheet electron density in the gated region of the channel is 1.93×10^{13}cm^{-2}. (b) without gate finger, but different sheet electron densities in the channel with the same coordinate as the gated channel in (a), 3.06×10^{13}cm^{-2} (green solid line), 1.82×10^{13}cm^{-2} (red dotted line), 0.56×10^{13}cm^{-2} (blue dashed line); the sheet electron density in the side channels is 1.82×10^{13}cm^{-2}. (c)The plasmon-induced electric field distributions along the channel of the device corresponding to the resonant peaks S_1, S_2, S_3, and S_4, as marked in Figs. 4(a)-4(b). The channel is located at the coordinate $Y = 1.20$ μm.

3.3. The field distributions of ungated SM plasmons, and ASM plasmons in gated and ungated channels

The gated and ungated plasmons mentioned above are the SM plasmons with dipole oscillation being confined along the 2D channel plane. In fact, the channel in the device is not really the two-dimensional system, especially for the one with thick quantum step. So it is possible to exhibit collective charge density oscillation vertically to the channel, so-called ASM plasmon in [33]. In the following, we consider the spectral characteristic of plasmons in the devices with the larger gate slits in Fig. 5.

Actually, the gated plasmons are not activated in Fig. 5 due to the broadening of the resonant line with larger gate slit. The resonant peaks with the frequency lower than 14THz are mainly dominated by the ungated plasmons, which are sensitive to the change of slit width (seeing the dashed line in Fig. 5(a)). And the frequency of these resonant peaks is not sensitive to the electron density under the gate or the gate voltage. The result is different from that in [20] and can be explained in Sec.3.4. Unlike the ungated plasmons, the resonant peaks marked as C_1 and C_2 can be tuned by the gate voltage, similar to that of the gated plasmons. Based on the field distribution under THz wave excitation, the types of dipole oscillations for

#182409 - $15.00 USD Received 2 Jan 2013; revised 17 Mar 2013; accepted 19 Apr 2013; published 25 Apr 2013

these two peaks are in agreement with the ASM plasmons as mentioned above. Moreover, the peak C_1 is related to the ASM plasmon in the gated channel, and the peak C_2 is related to the plasmon in the ungated channel.

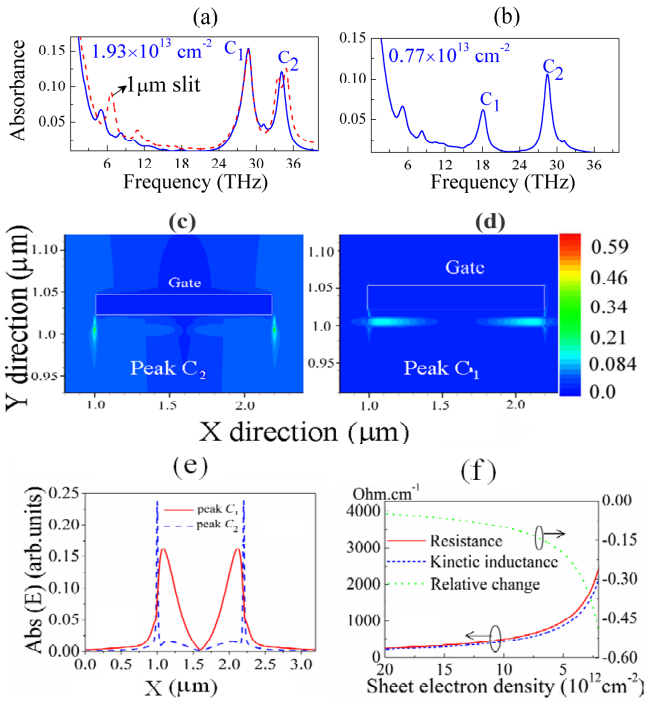

Fig. 5. (a) The plasmonic spectra of AlN/GaN HEMTs with 2μm slit and 1.2μm gate length, the sheet electron density in the gated channel of (a) and (b) is 1.93 × 10^{13}cm^{-2}, 0.77 × 10^{13}cm^{-2}, respectively. (c) and (d) show the plasmon-induced electric-field distributions along the channel, (c) the field distribution corresponding to the resonance C_2 of the ungated ASM plasmon, (d) the field distribution corresponding to the resonance C_1 of the gated ASM plasmon. (e) the field strength (Abs(E)) corresponding to ASM plasmons. (f) the kinetic inductance (blue dashed line) in the gated channel as a function of the electron density; and right axis, the relative change (green dotted line) of the resistance ($\Delta R_g/R_g$) and kinetic inductance ($\Delta L_g/L_g$) in the gated channel.

As referring to the tunability of these plasmons, it is related to the field distributions along the channel as depicted in Figs. 5(c)-5(e). We find the spreading of electric-field line over the side channels in Fig. 5(e), and thus the frequency of these plasmons is strongly affected by the electrical parameters along the side channels. By using the equivalent circuit model, as shown in [20], the reflection coefficient (the ratio of internal reflected and incident waves) at the interface between gated and ungated channels is given as follows:

$$\Gamma_{\text{ref}} = \frac{Z_g - Z_{ug}}{Z_g + Z_{ug}}, \tag{3}$$

where $Z_{g/ug} = \sqrt{\dfrac{R_{g/ug} + j\omega L_{g/ug}}{j\omega C_{g/ug}}}$ is the characteristic impedance in the gated and ungated channels, and $C_{g/ug}$ is the characteristic capacitance in the gated and ungated channel ($C_{g/ug}$~0.3pF/cm). Figure 5(f) shows the change in resistance R_g or kinetic inductance L_g with the sheet electron density in the gated region of the channel. The results indicate that the resistance or inductance increases dramatically when the channel is nearly pinched off (around 5 × 10^{12}cm^{-2}). This leads to the total internal-reflection (coefficient Γ ~1) of plasmon

#182409 - $15.00 USD Received 2 Jan 2013; revised 17 Mar 2013; accepted 19 Apr 2013; published 25 Apr 2013

at the interface between gated and ungated channels. Therefore, the frequency of ungated ASM plasmon can be tuned above threshold as shown in Figs. 5 (a) and 5(b).

From Fig. 5 we notice that ASM plasmon mainly locates on the higher order shoulder of SM plasmon, such phenomenon is similar to previous results appearing in [41] and [38]. The frequency of such plasmon in GaN HEMT is several times higher than that in [41] due to its potentially higher electron density. At the frequency higher than 10THz, the optical-phonon excitation by the incident wave cannot be neglected in GaN or the substrate which supports the entire device. The phonon absorption may cause the limits of these results to practical applications. As example, for sapphire substrate [42], there are four infrared active modes with dipole moment being perpendicular to the *c*-axis and the frequency interval between transversal and longitudinal optical vibration modes is from 14 to 30THz. Therefore, the contribution of resonance C may be covered with the zero transmission during the FTIR experiments [26]. Our recent results indicate that the reflection from substrate can enhance the strength of plasmon resonance significantly, and such mechanism is required to have further investigation. Thus, if one wants observe the ASM plasmon resonance in the thin channel layer with the frequency being higher than 10THz, it is necessary to reduce the absorption loss of phonons both in the buffer and substrate layers.

3.4. The tunability of resonance absorption of ungated plasmons in III-Nitride system

As shown in Sect. 3.3, no obvious frequency shift of ungated plasmons can be observed. However, in [20], the ungated plasmons exhibit obvious frequency shift as the gate voltage changes. In order to search the reasons for the deviation, we turn our attention to the device with shorter gate length (100nm), but the sizes of the ungated channel remain the same as that in Fig. 5. By scaling the length of the gate fingers, the plasmon-induced electric field at two sides of the gate finger can couple with each other, so that the effect of voltage modulation on the frequency of ungated plasmons may emerge. The results obtained are shown in Fig. 6(a). As expected, there is a significant frequency shift Δf of resonant peak *D* in the spectra of devices with or without the added gate, and plasmon resonance can be tuned from 1 to 4 THz through changing the gate voltage. These phenomena indicate that the tunability of the ungated plasmon can be improved by scaling the length of gate finger.

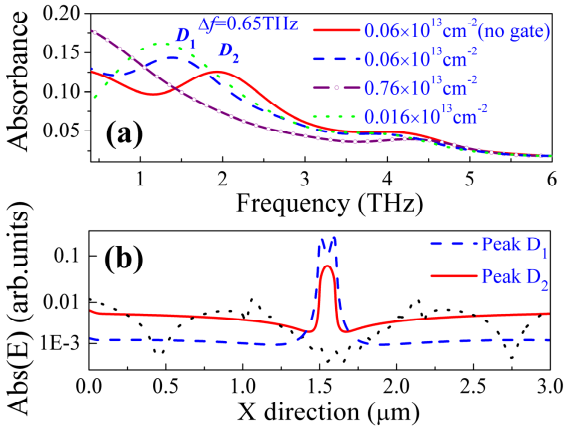

Fig. 6. The plasmonic spectra of the devices with short gate length (100nm) and the plasmon-induced electric field distribution along the channel, (a) the spectra of devices with 100nm gate length after varying the sheet electron density in the gated channel from 0.76 × 10^{13}cm^{-2} down to 0.016 × 10^{13}cm^{-2}. The spectrum of the device without gate added (red solid line in (a)) is also shown for convenience of comparison. A frequency shift $\Delta f = f(D_2)-f(D_1)$ is indicated near the peaks D_1 and D_2; (b) the plasmon-induced electric field distributions along the channel are extracted in correspondence to the peak D_1 (blue dashed line), peak D_2 (red solid line), and the fundamental ungated plasmon resonance in the device with 1.2μm gate length (black dotted line) in Fig. 5. The sheet electron density in the ungated channel is 1.82 × 10^{13}cm^{-2} in these figures.

#182409 - $15.00 USD Received 2 Jan 2013; revised 17 Mar 2013; accepted 19 Apr 2013; published 25 Apr 2013

For better visualization, the plasmon-induced field distribution along the channel is shown in Fig. 6(b), stronger field coupling occurs at the two sides of the electrode after scaling the length of gate finger, while the weak coupling strength in long gate device leads to the poor tunability. It should be noted that there is significant near-field enhancement with the enhancement-factor (E_{gated}/E_0, where E_0 is the amplitude of incident wave) exceeding 100 for the device with 100nm gate length. The result also indicates the strong electromagnetic energy pumping at the plasmonic cavity as confined by the side channels. This may have important application in improving the efficiency of the photo-detection for the inter-subband transition in quantum-dot systems. To fully explore the capability of cavity-pumping and tunability of the ungated plasmons, it is necessary to investigate the plasmonic spectra of devices with different gate finger length and gate bias. They will be discussed in our future work.

4. Conclusions

We have investigated the plasmon resonances in AlN/GaN HEMT devices with the following aspects, (i) the THz absorption properties of gated and ungated SM plasmons in devices with different sizes, (ii) the dynamic properties of gated and ungated SM plasmons at the anti-crossing regime of frequency dispersion, (iii) the tunability of ungated SM plasmons and ASM plasmons in gated and ungated channel, and (iv) the property of field-coupling between ungated plasmons. Our results indicate that the strength of plasmon resonance is increased when the two plasmons are commonly excited. However, the splitting of plasmon resonance is hardly observed at such a regime due to the in-phase charge oscillating across the boundary between gated and ungated channels. Except for the ungated SM plasmons, the ASM plasmon with wider frequency tunability can also be excited in the ungated channel. In regard to the tunability of the ungated SM plasmons, it is indicated that the field coupling between these plasmons at two sides of gate finger plays an important role. In the devices with a short gate length, significant near-field enhancement with an enhancement factor greater than 100 can be reached due to the strong cavity pumping of electromagnetic energy. The property may have important application in improving responsivity of quantum-structure detection system.

Acknowledgments

The authors acknowledge the support provided by the State Key Program for Basic Research of China (2013CB632705, 2011CB922004), the National Natural Science Foundation of China (10990104, 61006090, 61290301, 11274331), the Fund of Shanghai Science and Technology Foundation (10JC1416100), and Shanghai Rising-Star Program.